Natural Hazards (2023) 118:1855–1879
https://doi.org/10.1007/s11069-023-06017-7

ORIGINAL PAPER

Quantitative evaluation of flood damage methodologies under a portfolio of adaptation scenarios

Julien Boulange[1,2] · Yukiko Hirabayashi[1] · Masahiro Tanoue[3] · Toshinori Yamada[1]

Received: 19 October 2022 / Accepted: 11 May 2023 / Published online: 23 July 2023

Abstract

Flood risk is anticipated to increase, driven by climate change and socioeconomic development. Flood impact assessments rely heavily on models, and understanding the effects of uncertainties encompassed in the modelling chain is critical to adequately interpret flood risk and the development of effective flood adaptation measures. Previous research has focused on the effects of processes embedded in models, and flood frequency analysis of flood risk. However, no study has yet evaluated the cascading effects of flood damage assessment methodologies on uncertainty in the estimation of expected annual damage (EAD), optimal flood protection, and residual flood damage (RFD). Here, using an updated global river and inundation model forced by the latest climate data and employing a standard flood methodology, we found that global EAD will increase by $16.2 (USD throughout) and $44.5 billion yr^{-1} during 2020–2100 under low- and high-emissions scenarios, respectively. During the same period, despite the adoption of optimal levels of flood protections, global total RFD remained high under both low- and high-emissions scenarios, at $25.8 and $36.2 billion yr^{-1}, respectively. Our results demonstrate that, under current levels of flood protection, EAD will approximately double with a switch in methodology. Aggregating data at the regional scale revealed conflicting trends between methodologies for developing and high-income countries, driven by existing levels of flood protection as well as the intensity, evolution, and distribution of gross domestic product at the administrative unit scale. Flood damage methodology is the dominant source of uncertainty, followed by unit construction cost and discount rate.

Keywords Flood · Expected annual damage · Residual damage · Adaptation

✉ Julien Boulange
boulange@go.tuat.ac.jp

[1] Graduate School of Engineering and Science, Shibaura Institute of Technology, Tokyo, Japan

[2] Division of International Environmental and Agricultural Science, Tokyo University of Agriculture and Technology, Fuchu, Japan

[3] Meteorological Research Institute, Meteorological Agency, Tsukuba, Japan

1 Introduction

Long-term observations and model simulations both strongly suggest that global warming is already affecting the climate (Paik et al. 2020; Dong et al. 2021) and the hydrological cycle (Pörtner et al. 2022). Societies are particularly strongly impacted by changes in extreme events, as clearly demonstrated by devastating heatwave (D'Ippoliti et al. 2010; Lewis and Karoly 2013; Campbell et al. 2018) and drought (Kelley et al. 2015; Mann and Gleick 2015) events over the last decade.

Accounting for approximately 43% of global natural disasters, flood-related disasters are highly disruptive, with the potential to affect multiple countries simultaneously and cause serious damage worldwide (Jongman et al. 2014; Dottori et al. 2018). At present, approximately 0.8 billion people and 50 trillion US dollars in assets are exposed to 1-in-100-year river flood events annually (Jongman et al. 2012). Changes in climate driven by anthropogenic emissions are already affecting floods (Blöschl et al. 2019; Hirabayashi et al. 2021a), increasing economic losses associated with flooding in many parts of the world. Multiple independent studies that have employed a wide range of models, input data, and methods have overwhelmingly found that flood risk will increase in the future, driven by changes in climate, land use, and socioeconomic conditions (Dottori et al. 2018; Hirabayashi et al. 2021b; Taguchi et al. 2022). Population exposure to the historical 1-in-100-year river flood level is anticipated to increase in proportion to the degree of warming and could reach 1.4-fold the historical exposure level to 1-in-100-year river floods, given 3 °C of warming (Hirabayashi et al. 2021b).

Several global databases of flood protection measures have emerged in recent years (Scussolini et al. 2016; Wing et al. 2019). Integrating these databases into flood assessments is essential to obtain realistic estimates of flood exposure and flood damage (Winsemius et al. 2016). For example, a recent study demonstrated that spending approximately $6.8 billion for flood adaptation could reduce annual flood damage by approximately $74 billion by 2100 and would be particularly effective in China, India, and Latin America (Tanoue et al. 2021). The same analysis noted that flood damage exceeding 0.1% of gross domestic product (GDP) remains a risk in eastern China, northern India, and central Africa despite the consideration of adaptation measures. A study focused on Europe revealed that increasing flood protection levels in all basins to a minimum of the 1-in-100-year river flood level would decrease total annual losses associated with flood by about €7 billion (by 2050) while only costing approximately €1.75 billion (Jongman et al. 2014). At the global scale, spending $78 billion on global adaptation would reduce annual flood damage by $79.9 billion from 2020 to 2100 (Ward et al. 2017). Other studies have endorsed the integration of flood protection measures into flood studies (Ward et al. 2013; Boulange et al. 2021; Hanazaki et al. 2022; Chaudhari and Pokhrel 2022).

Given the limited spatiotemporal coverage of flood observations, flood impact assessments rely heavily on global flood hazard model (GFHM) simulations. Consequently, understanding the effects of cascading uncertainties, which are linked to the modelling chain employed (e.g., climate models, future scenarios, and flood models), is critical to the adequate interpretation of flood risk and the development of effective adaptation actions (Zhou et al. 2021; Meresa et al. 2021). Despite the importance of quantifying uncertainty in flood risk analysis and a call to make uncertainty analysis mandatory in flood damage assessments (Merz et al. 2010), only about one sixth of existing flood studies have incorporated an uncertainty framework (Díez-Herrero and Garrote 2020).

Future flood assessments typically account for multiple climate forcings using an ensemble of climate models (Kundzewicz et al. 2014). Such studies focus on a limited subset of variables that are key to determining flood characteristics, such as precipitation (Rözer et al. 2019; Mei et al. 2020), runoff, river streamflow conditions (Zhao et al. 2017; Zhou et al. 2021), sea level rise, storm properties (Vousdoukas et al. 2018a, b; Marsooli et al. 2019; Rasmussen et al. 2020), and the rainfall–runoff–storm relationship (Bevacqua et al. 2019; Xu et al. 2023) in the contexts of urban, river, coastal, and compound flooding. In addition, the importance of assumptions regarding socioeconomic development and flood protection standards in assessments of future flood risk is widely recognized (Winsemius et al. 2016; Ward et al. 2017; Sauer et al. 2021; Kirezci et al. 2023). Molinari et al. (2019) suggested that common practices for validation of flood risk models should be developed, as estimates of flood inundation area, economic losses and exposed population vary strongly and significantly among models (Trigg et al. 2016). This variability has prompted researchers to suggest the use of an ensemble of flood risk models for large-scale flood assessment whenever possible (Winsemius et al. 2013; Devitt et al. 2021). Yamazaki et al. (2014) noted that differences in simulated river streamflow and inundation area among GFHMs are magnified in deltaic regions where branch flow processes strongly influence flood simulation results. These uncertainties propagate to the estimates of population exposed to flood risk, which can differ by up to 14% depending on the physical processes considered in the GFHMs and the input data employed (Yamada et al. 2021). Likewise, elevation data have been reported to be a critical source of uncertainty in urban, river, and coastal flood studies, with the potential to triple estimates of global vulnerability to sea level rise and coastal flooding (Yamazaki et al. 2019; Kulp and Strauss 2019; Arrighi and Campo 2019). Flood analyses rely on extreme value theory to derive flood return periods, which is a critical source of uncertainty that directly influences flooded water depth and inundation area (Chavez-Demoulin and Davison 2012; Hirabayashi et al. 2013, 2021b; Zhou et al. 2021). The damage component of flood risk analyses relies on depth–damage curves, which define the percentage of the value of assets damaged as a function of flood depth. However, the large discrepancy in building materials and construction quality among communities severely limits their applicability in spatial and temporal terms (McGrath et al. 2019; Lüdtke et al. 2019; Wing et al. 2020; Kirezci et al. 2023), limiting the application of flood risk assessment.

Numerous studies have derived historical and future flood damage at global (Merz et al. 2010; Winsemius et al. 2016; Dottori et al. 2018; Tanoue et al. 2021), continental (Johnson et al. 2020; Davenport et al. 2021), and local scales (Shrestha et al. 2019; Romali and Yusop 2020). Over the past 5 years, Web of Science has indexed a total of 1,218 articles related to flood damage that directly incorporated one or more methods, approaches, or techniques related to hazard (e.g., hydrology, geosciences, and paleo-hydrology), exposure (e.g., population and land use), vulnerability (e.g., social vulnerability, economic vulnerability, and damage functions), and other (e.g., cost–benefit analysis and susceptibility analysis). All of these components and associated keywords are defined in Díez-Herrero and Garrote (2020). Approximately 64% of these articles focused on only one component of flooding (Fig. 1a). The remaining articles generally incorporated two components, usually a combination of exposure, vulnerability, and other categories (Fig. 1b). Among 194 articles that utilized a cost–benefit methodology for flood damage assessment, less than half considered multiple flood components in their analysis. Moreover, the few studies that computed residual flooding relied on outdated climate projections and did not report the effect of cascading uncertainty embedded in flood damage assessment methodology on

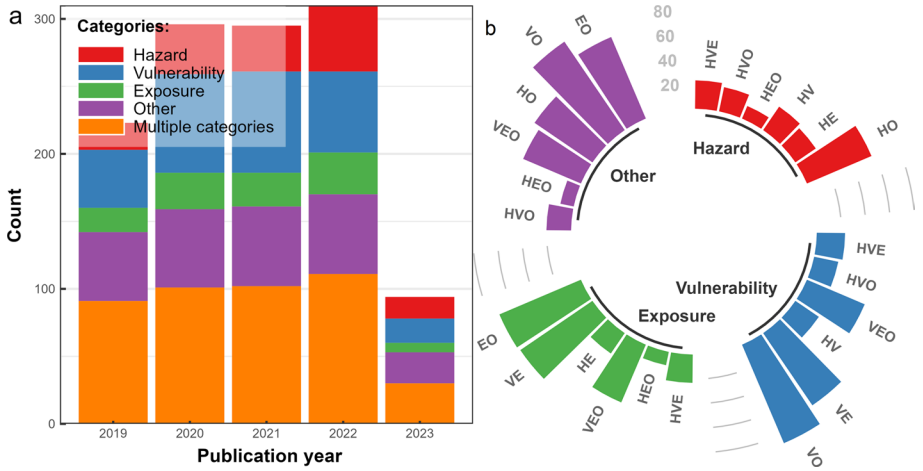

Fig. 1 Articles indexed by Web of Science dedicated to flood damage and incorporating one or more methods, approaches, and techniques related to hazard, exposure, vulnerability, and other components, as defined by Díez-Herrero and Garrote et al., (2020). **a** Articles from the past 5 years focusing on "flood damage" are classified based on methods, approaches and techniques. **b** A meticulous examination and classification of articles integrating multiple components of hazard (H), exposure (*E*), vulnerability (*V*), other (*O*). Search performed on March 27th, 2023

estimated annual damage, optimal flood protection, and residual flood damage, leaving a gap in our understanding.

In this study, we assessed annual flood damage, optimum flood protection levels, and associated residual flood damage using two established flood damage methodologies under a portfolio of adaptation scenarios. Forcing an updated global river and inundation model with the latest climate simulations, we attribute the overall uncertainty to four sources including flood assessment methodology and three key economic assumptions.

2 Materials and methods

2.1 Forcing data

2.1.1 Retrospective simulation

The bias-corrected reanalysis dataset S14FD (Iizumi et al. 2017) was used in conjunction with the land surface process model MATSIRO (Takata et al. 2003) to generate daily runoff values (Fig. 2). The S14FD product, spanning 1958–2013, is derived from the JRA-55 reanalysis data (Harada et al. 2016). Despite neglecting the effect of anthropological activities on the water cycle, correction for monthly biases in precipitation, vapor pressure, and absolute humidity, among other variables, allows the S14FD product to skillfully reproduce observed extremes of temperature and precipitation (Iizumi et al. 2017). The daily runoff data (0.5-degree spatial resolution) are used as forcing input data for the CaMa-Flood model. Our goal was to establish a trustworthy relationship or lookup table, between the return period associated with floodwater volume and, inundated area at a fine

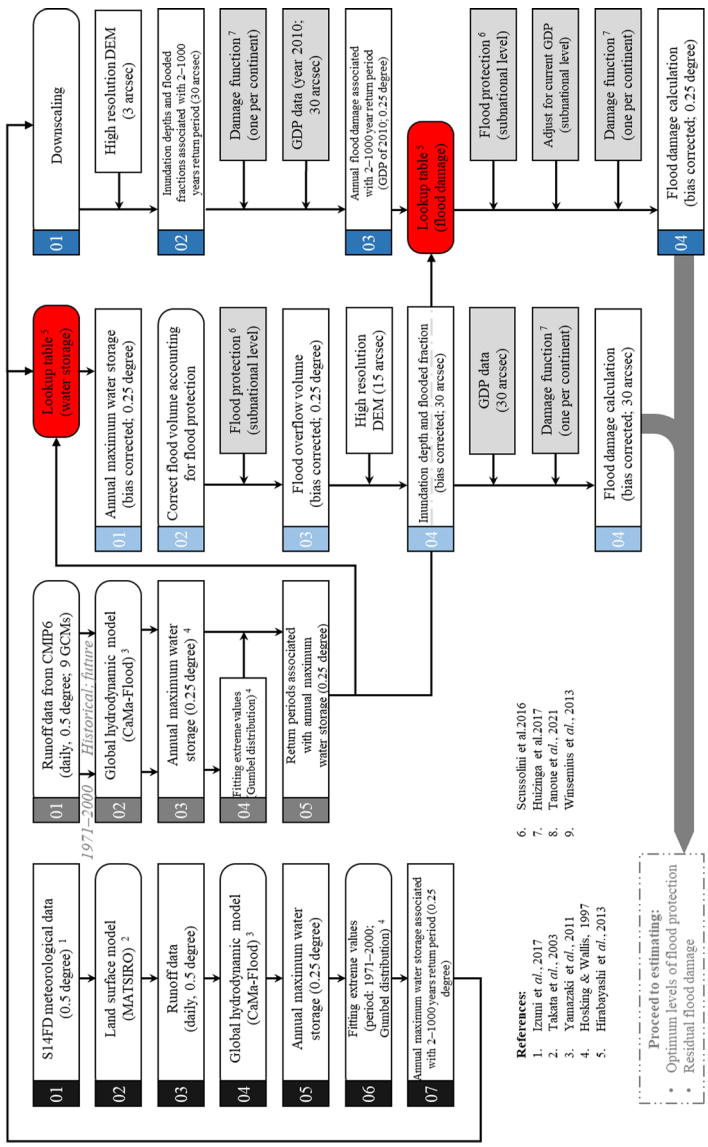

Fig. 2 Flowchart illustrating the steps involved in calculating flood damage using two distinct methods. Spatial and temporal resolutions of the various datasets are provided

spatial resolution of 3 arcsec (Fig. 2). This framework was previously successfully used to reproduce observed historical streamflow and inundation area in Thailand (Tanoue et al. 2020; Taguchi et al. 2022).

2.1.2 Acquisition of daily historical and future runoff data

Daily runoff products from atmosphere–ocean general circulation models (AOGCM) were acquired directly from the Coupled Model Intercomparison Project Phase 6 (CMIP6; Eyring et al. 2016). Applying the same rationale and methods as Hirabayashi et al. (2021b), we selected nine AOGCMs from independent institutions and harmonized the provided gridded runoff data to a common 0.5-degree grid using bilinear interpolation. Runoff products from CMIP6 can be divided into two periods, historical and future, which span 1960–2014 and 2015–2100, respectively. Future runoff estimates were further subdivided into Shared Socioeconomic Pathway–Representative Concentration Pathway (SSP–RCP) scenarios, interweaving plausible climate and societal future scenarios. Here, we limit our analysis to two scenarios, ssp126 and ssp585, representing a rapid transition to a sustainable society paired with low greenhouse gas concentrations and a resource-hungry society that relies on fossil fuels paired with high greenhouse gas concentrations, respectively. Note that at the time we archived the data, one of the AOGCMs was not available for the ssp126 scenario and the ensemble was composed of the remaining eight AOGCMs (Supplementary Table 1). Although the high-emissions scenario has faced criticism, due to its implausible assumptions regarding coal use (Ritchie and Dowlatabadi 2017), it has the advantage of clearly showing the trend of flood impacts and was therefore adopted in this study.

2.2 Global hydrodynamic model

The global river routing model used in conjunction with the forcing data presented above is the latest version of the catchment-based macroscale floodplain model (CaMa-Flood v4.0; Yamazaki et al. 2011, 2014). The CaMa-Flood model employs a vector-based representation of the river network that optimally represents sub-basin connectivity and is computationally efficient. Efficiency is critical in global flood studies, as the large ensemble simulations that are necessary to account for climate uncertainties rapidly increase computation time.

The fundamental hydrographic dataset, MERIT-Hydro (Yamazaki et al. 2019) is primarily based on the combination of Multi-Error-Removed Improved-Terrain digital elevation model (DEM; Yamazaki et al. 2017), which was improved through the removal of various observation errors, with the Flexible Location of Waterways (FLOW) method (Yamazaki et al. 2009). At present, MERIT-Hydro provides the most accurate representation of river networks as demonstrated in multiple independent analyses (Getirana et al. 2021; Eilander et al. 2021).

In CaMa-Flood, water dynamics in the floodplain are realistically simulated by explicitly solving the local inertia equation (Bates et al. 2010), thereby representing backwater effects. Water storage is the only prognostic variable and is acquired by solving the water balance equation. Other variables, such as inundation area and inundation depth, are determined by dividing river networks into unit catchments and combining water storage

with other relevant topographic parameters (Yamazaki et al. 2011). The CaMa-Flood model faithfully reproduces historical flood patterns (Yamazaki et al. 2011, 2012, 2014) and largely outperforms global hydrological models for reproducing historical streamflow (Zhao et al. 2017).

A new addition in CaMa-Flood v4.0 is the introduction of satellite-based estimation of river geometry (Yamazaki et al. 2019). The empirical method previously employed to estimate river geometry (Yamazaki et al. 2011) has been updated (Yamazaki et al. 2019) but is relegated to deriving river geometry where satellite observations are not available. The CaMa-Flood model is modular, allowing users to activate or deactivate specific features. In our simulations, we activated both discharge from floodplains and the channel bifurcation scheme. All simulations were performed globally, and the output consisted of daily total water storage at 15-arcmin spatial resolution (approximately 25 km at the equator). The simulation periods were 1953–2013 for the runoff products produced with MATSIRO and 1960–2100 for the runoff input obtained from CMIP6, respectively. A spin-up period of 5 years was completed prior to the historical simulations. For future simulations, no spin-up was necessary, as the simulations were initialized using the water storage conditions obtained from historical simulations.

2.3 Flood impact analysis

2.3.1 Global river flood simulation

As the simulations are directly forced by runoff from AOGCMs without correction of bias, inundation areas and inundation depths are not determined directly in CaMa-Flood simulations. Instead, we associated the recurrence frequency (return period) of the predicted annual maximum water storage in each grid (15 arcmin) with inundation area and inundation depth at a fine spatial resolution (30 arcsec, approximately 1 km at the equator) using retrospective simulations (see Sect. 2.1.1).

The annual maximum water volumes obtained from the retrospective simulation during 1971–2000 were fitted to a Gumbel distribution (Gumbel 1941) using the L-moments method (also called probability weighted moments) due to its reliability for relatively small size samples (Greenwood et al. 1979; Hosking and Wallis 1997). The established Gumbel distributions were subsequently used to estimate the annual maximum water volume associated with 2- to 1000-year return periods in all grid cells (15 arcmin), which form the basis of the lookup tables (Fig. 2). Note that all equations and intermediate steps used to estimate the two parameters of the Gumbel distribution are provided in the supplementary documents of Hirabayashi et al. (2013, 2021b).

The procedure employed in the flood simulations based on CMIP6 runoff begins identically to that described above for the retrospective simulation (Fig. 2). After forcing of the CaMa-Flood model with CMIP6 runoff data, we extracted annual maximum water volumes for the period of 1971–2000 and fit a Gumbel distribution using the methodology noted above. The fitted distribution was subsequently applied to the future period (2015–2100) to assess the return period associated with annual maximum water volumes in each grid cell and year. Finally, we adjusted for bias in climatic hydrological variables obtained from the AOGCMs using the lookup tables established based on the retrospective simulation, converting return periods associated with flooding to inundation depths or flood damage, depending on the flood methodology adopted (see Supplementary Figs. 1 to 3).

2.3.2 Flood damage

We compared two established but distinct methods for deriving historical and future flood damage. While the procedural steps for deriving flood damage differ between the two methods, flood damage is nevertheless consistently defined as the product of hazard, exposure, and vulnerability (Winsemius et al. 2013). Exposure consists of gridded GDP maps representing present and future socioeconomic conditions derived using the methodology proposed by Tanoue et al. (2021). Vulnerability is expressed as the combination of flood protection levels (FLOPROS) and damage functions, with the latter describing the relationship between inundation depth and damage severity across continents (Huizinga et al. 2017). Furthermore, all subsequent analyses involving the estimation of flood damage, such as residual flood damage and adaptation costs and benefits, are identical in the two methods (Fig. 2).

Method 1 employs the magnitude of flooding, the value of assets, and the level of flood protection to represent the hazard, exposure, and vulnerability, respectively (Tanoue et al. 2021). The eventual presence of flood protection is considered immediately, assuming that a flood with a return period shorter the design period of the local flood protection is fully mitigated. Hence, in such locations, the inundation depth and flooded fraction are zero. In contrast, in locations where the return period of a flood is longer than the local flood protection (i.e., where the flood magnitude exceeds the local protection level), we calculated the volume of overflowing floodwater and then downscaled this volume to high-resolution inundation depth and flooded fraction (Fig. 2). Method 1 is not widely applied to riverine flood assessments, possibly due to the additional computational cost involved in calculating overflow volume. Nevertheless, an analogous technique has been employed in multiple coastal flood assessments (Vousdoukas et al. 2018a, c).

Method 2 has been used in multiple urban and riverine flood risk assessments (Winsemius et al. 2013; Hallegatte et al. 2013; Dottori et al. 2018, 2023). In method 2, flood volume is not adjusted for the eventual presence of flood protection; hence, this method is less resource-intensive than method 1. The first step of method 2 involves the derivation of accurate lookup tables linking flood damage to the magnitude of floods (2- to 1000-year return periods; Fig. 2). These tables are constructed by downscaling the annual maximum water storage associated with 2- to 1000-year return periods from the retrospective simulation (Fig. 2) onto a high-resolution DEM (See Supplementary Figs. 1 and 2). Then, flood damage tables are obtained by upscaling the available maps to a resolution of 30 arcsec for overlaying exposure (GDP in year 2010; see supplementary Fig. 3) and vulnerability (damage function) information. Finally, annual flood damage is computed by converting flood return periods into flood damage using the tables described above with adjustment for future changes in GDP. In this step, biases originating from climatic variables are effectively removed.

As demonstrated above, the definition of flood damage is consistent in both methods. To simplify the interpretation of this analysis, we highlight some key differences between the two methods. First, method 1 is based on the overflow volume of floodwater, whereas method 2 is based on the total volume of floodwater. Consequently, flood damage is anticipated to be greater with method 2 compared to method 1. Second, the downscaling of floodwater relies on DEM with different spatial resolutions, which can be expected to result in lower damage with method 2 due to the more accurate redistribution of floodwater. Third, the lookup tables used in method 2 rely on GDP distribution data from 2010, meaning that only the intensity of GDP is scaled annually, rather than both its intensity and

distribution, as in method 1. For countries experiencing high GDP growth (Supplementary Fig. 7), the future spatial distribution of GDP could be very different from that in 2000, directly affecting EAD calculation. Nevertheless, because we report our results globally, for the World Bank regions, and for administrative levels, this future GDP distribution cannot be responsible for any differences in flood damage between the two methods.

2.4 Estimation of current and future flood protections

Existing flood protection data were acquired from the FLOPROS database (Scussolini et al. 2016), which provides, globally and at the administrative level, the flood return periods associated with protection measures. FLOPROS was created by merging three distinct layers of information. The design layer provides empirical data about the actual standard of existing flood protection measures. The policy layer includes information on flood protection standards as mandated by regulations and policies. Finally, the model layer estimates flood protection levels using a combination of flood hazard modelling and the relationship between wealth and flood protection. When these layers are combined, the design layer, which contains the most reliable and accurate information on actual flood protection measures, is prioritized. If no data are available from the design layer, the policy layer, which provides information about the minimum standards of flood protection required by regulations and policies, is used. Finally, the model layer is used only when no other information is available. Current levels of flood protection provided by FLOPROS are particularly reliable for European countries and China. In contrast, the model layer provides information over most of Africa, South America, and large parts of Russia.

Future flood protection levels were derived following the established relation: $\mathrm{FPL}_{\mathrm{future}} = \mathrm{FPL}_{\mathrm{current}} \times 2^{L}$ where $\mathrm{FPL}_{\mathrm{future}}$ and $\mathrm{FPL}_{\mathrm{current}}$ represent future and current flood protection levels, respectively. The adaptation level, represented by L, increases gradually by 0.25 over the interval 0–10, resulting in the derivation of a maximum of forty protection levels, as $\mathrm{FPL}_{\mathrm{future}}$ is capped at 1000 years (Tanoue et al. 2021). The total adaptation cost associated with all future protection levels is calculated based on the unit construction cost, fixed at \$2.399 million per km per $\log2(\mathrm{FPL}_{\mathrm{future}})$; operation and maintenance cost, set at 1% of the construction cost associated with the project; and an assumed 5% discount rate for all subnational administrative units (Supplementary Table 2). This framework was established by Tanoue et al. (2021) based on information about cost and protection levels aggregated from 256 international flood protection projects. For each of the future protection levels, we calculated future EAD and conducted a cost–benefit analysis to determine the scenario maximizing the difference between benefits and adaptation costs, at the administrative level. Under this optimized adaptation scenario, flood protection remains relatively affordable while the protection of assets is maximized. Benefits are quantified as the reduction in EAD between simulation considering an adaptation scenario and the default simulation assuming current levels of flood protection. RFD is defined as the difference between the future and present EAD (1971–2000), adjusted for eventual socioeconomic development (Tanoue et al. 2021). Critically, we performed additional analyses using selecting alternative unit construction costs, operation and maintenance costs, and discount rates (Supplementary Table 2). Because no alternative data regarding unit construction cost are available, we explored the impacts of halving and doubling the default unit construction cost on our analysis. Likewise, two alternative maintenance rates (3% and 5% of the construction cost) were selected. Finally, discount rates used in previous flood analyses typically range between 8%, the Chinese official discount rate, and 4%,

corresponding to the interbank lending rates in Shanghai (Du et al. 2020). We determined the influence of the discount rate by assigning values of 0, 1, 2, 3, and 8%. Performing additional cost–benefit analyses with these alternative values allowed us to quantitatively and comprehensively investigate the cascading effect of uncertainty embedded in these parameters on the determination of EAD, optimal flood protection levels, and RFD.

2.5 Decomposition of variance

We applied four-way multifactorial analysis of variance (ANOVA) to changes in future levels of flood protection to decompose the variance. Four main factors were established, namely, flood damage method, discount rate, unit construction cost, and maintenance cost, as they were reported to be primary causes of variance in flood damage assessment (Tanoue et al. 2021). ANOVA was conducted at the administrative level, which is compatible with the levels of current and future flood protection. The total sum of squares (TTS) is expressed as Eq. 1 (Hattermann et al. 2018; Satoh et al. 2021):

$$\mathrm{TSS} = \sum_{i=1}^{N_{\mathrm{met}}} \sum_{j=1}^{N_{\mathrm{dis}}} \sum_{k=1}^{N_{\mathrm{mat}}} \sum_{l=1}^{N_{\mathrm{mai}}} \left(X_{\mathrm{ijkl}} - \overline{X} \right) \tag{1}$$

where X_{ijkl} is the specific value for a subnational unit corresponding to flood damage i, discount rate j, unit construction cost k, and maintenance rate l; $\overline{X}$ is the overall mean; and N is the number of samples for a factor. The main factors are denoted with the subscripts *met*, *dis*, *mat*, and *mai*, indicating flood damage method, discount rate, unit construction cost, and maintenance cost, respectively. TTS can be further decomposed into four main effects and ten interaction terms, representing all interactions among flood damage method, discount rate, unit construction cost, and maintenance cost:

$$\begin{aligned} \mathrm{TSS} = {} & \mathrm{SS}_{\mathrm{met}} + \mathrm{SS}_{\mathrm{dis}} + \mathrm{SS}_{\mathrm{mat}} + \mathrm{SS}_{\mathrm{mai}} + \mathrm{SS}_{\mathrm{met}*dis} + \mathrm{SS}_{\mathrm{met}*\mathrm{mat}} \\ & + \mathrm{SS}_{\mathrm{met}*mai} + \mathrm{SS}_{\mathrm{dis}*\mathrm{mat}} + \mathrm{SS}_{\mathrm{dis}*\mathrm{mai}} + \mathrm{SS}_{\mathrm{mat}*\mathrm{mai}} \\ & + \mathrm{SS}_{\mathrm{met}*\mathrm{dis}*\mathrm{mai}} + \mathrm{SS}_{\mathrm{dis}*\mathrm{mat}*\mathrm{mai}} + \mathrm{SS}_{\mathrm{met}*\mathrm{dis}*\mathrm{mat}*\mathrm{mai}} \end{aligned} \tag{2}$$

where *SS* is the sum of squares and suffixes indicate the main factors involved in an interaction term. The main factor effect (*SS*) and contribution (*CR*) of the flood damage method to the overall variance can be calculated using Eq. 3 and 4, respectively:

$$\mathrm{SS}_{\mathrm{met}} = N_{\mathrm{dis}} N_{\mathrm{mat}} N_{\mathrm{mai}} \sum_{i=1}^{N_{\mathrm{met}}} \left(\overline{X_i} - \overline{X} \right)^2 \tag{3}$$

$$\mathrm{CR}_{\mathrm{met}} = {}^{\mathrm{SS}_{\mathrm{met}}}/_{\mathrm{TSS}} \tag{4}$$

where $\overline{\mathrm{X_i}}$ is the mean across indices (consistent with Eq. 1) j, k, and l for flood damage method i. The main factor effect and contribution to overall variance of the remaining main effects can be computed using equations analogous to Eqs. 3 and 4 and equations for the interaction terms are provided in the supplementary materials (Supplementary Equations).

3 Results and discussion

3.1 Historical and future flood damage under current flood protection levels

On average, EADs caused by floods during 1971–2000 estimated from the retrospective simulations were $58.5 (20.4–117.0; 5th–95th confidence interval given hereafter unless otherwise specified) and $27.9 (11.0–50.7) billion per year (2005 purchasing power parity basis) for methods 1 and 2, respectively. The same retrospective simulation conditions with a previous version of the CaMa-Flood model and method 1 were previously employed by Tanoue et al. (2021), who reported EAD of $62 billion in 1961–2013. The EADs obtained using methods 1 and 2 accounted for 0.14% (0.04–0.28) and 0.082% (0.02–0.12) of GDP in 2010, respectively. Overall, these estimates are well within the range of 0.044–1.6% reported in the literature (Winsemius et al. 2016; Alfieri et al. 2017; Kinoshita et al. 2018; Dottori et al. 2018; Tanoue et al. 2021). For 1971–2000, EAD estimates obtained with method 1 are systematically higher than those calculated using method 2. In addition, both urban and rural EADs estimated using method 1 are approximately double those estimated using method 2. We aggregated the EADs obtained in the retrospective simulation using the seven regions defined by the World Bank (see Supplementary Fig. 4 for the delineation of World Bank regions; Supplementary Fig. 5a). This analysis revealed that the largest differences in EAD estimates between the two methods occurred over the regions of East Asia and Pacific, Europe and Central Asia, and North America. The differences in EADs obtained with the two methods using the same input data (retrospective simulation, CMIP6) stem from the number of flood events that induce damage each year (Supplementary Fig. 5b). Those numbers varied substantially between methods; for example, in the Europe and Central Asia region during 1971–2000, averages of 1281 and 287 flood events causing monetary damage per year were detected using methods 1 and 2, respectively. The downscaling of floodwater stage dictates the number of flood events causing monetary damage. As noted above, DEMs of different resolutions (Fig. 2) were used for downscaling due to computational cost, and the higher-resolution DEM used in method 2 substantially reduces flood damage in economically developed areas.

Next, we investigated the evolution of EAD without considering any further adaptations to flood risk using the current flood protections listed in the FLOPROS database (Scussolini et al. 2016). As depicted in Fig. 3a, the differences between global-scale EADs reported using the two methods are substantial. During 2020–2100 under the ssp585 scenario, EAD increased by approximately $44.5 (42.6–46.4) and $90.3 (85.3–95.2) billion per year for methods 1 and method 2, respectively. In contrast, during the same period under the ssp126 scenario, the annual increase in EAD was much smaller, at $16.2 (15.5–16.9) and 31.1 (29.7–32.4) billion per year for methods 1 and 2, respectively. Clearly, at the global scale, EADs computed using method 2 are systematically higher than those obtained using method 1. These differences tend to be small at first but increase steadily in the future under the high-emissions scenario (Fig. 3a). Under the low-emissions scenario, the EADs projected with the two methods had similar magnitude, but those obtained with method 2 were larger than those computed using method 1, consistent with previous observations. Next, we briefly compare these results with a previous study (Tanoue et al. 2021). Despite substantial development of AOGCMs, the patterns in flood frequency were similar within CMIP5 and CMIP6, as differences in the direction of change affect limited regions in which the agreement regarding the direction of change in flood frequency is low among AOGCMs (Hirabayashi et al. 2021b). Consequently, although the CMIP product version

Fig. 3 Expected annual damage (EAD) from flooding under current level of flood protection. **a** Global EAD for the two methods and two scenarios. The color bands represent the first and thirst quartiles range from AOGCMs. **b** Average EAD under ssp585 scenario between 2071 and 2100, aggregated for the seven World Bank regions

and number of AOGCMs employed in this study and Tanoue et al. (2021) differed (5 and 9 AOGCMs, respectively), these factors were unlikely to explain the large differences in EAD obtained using a common flood damage methodology (method 1; see Fig. 3a). Alternatively, these differences are likely to result from the use of different simulation settings and versions of the global river routing model (v3.9.3 vs. v4.0). Specifically, our simulations relied on an updated, more accurate DEM and activation of the bifurcation scheme, both of which greatly improved the reproduction of flood dynamics in deltaic regions (See Sect. 2.2; Yamazaki et al. 2014; Yamada et al. 2021).

The trends discussed above at the global scale are not necessarily observed after aggregation of EADs using the seven regions defined by the World Bank (Fig. 3b). Regardless of the flood damage method employed, EADs are particularly high over the regions of South Asia, East Asia and Pacific, and Sub-Saharan Africa, as the current level of flood protection (obtained from FLOPROS; see Supplementary Fig. 6) in these regions is rather low. In general, EADs estimated in the previous study (using CMIP5, method 1, and CaMa-Flood v3.9.3) were highest, consistent with global-scale aggregation (Fig. 3a), particularly over the South Asia and East Asia and Pacific regions (Fig. 3b). Previous research has highlighted the importance of an accurate DEM and representation of mega deltas for accurate flood simulation in such regions (Yamazaki et al. 2014, 2017). Likewise, the use of different DEMs and the activation of various options embedded in CaMa-Flood have been reported to strongly influence the estimate of population exposed to flood risk (Yamada et al. 2021). Comparing methods 1 and 2, the EADs calculated using method 2 are far greater than those obtained with method 1 in low-income economies such as South Asia, Sub-Saharan Africa and much of the East Asia and Pacific region (Fig. 3b). As briefly discussed in the methods section above, only overflow floodwater is used to assess flood exposure and derive flood damage with method 1. In contrast, when the flood frequency exceeds the level of local flood protection, the latter is assumed to be breached; therefore, all water stored in the floodplain contributes to the exposure assessment and derivation of flood damage in method 2. The EADs calculated with method 2 were substantially lower than EADs obtained using method 1 in high-income economies such as Europe and Central Asia and North America. Current levels of flood protection are high in these regions (supplementary Fig. 6), mitigating minor flood events. The volumes of floodwater originating from major flood events (i.e., those with recurrence periods higher than the level of flood protection) are downscaled in both flood damage methods. The high-resolution (3 arcsec) DEM used in method 2 accurately redistributes floodwater. Method 1 does not rely on the same high-resolution DEM due to prohibitive computational cost, and a lower-resolution (15 arcsec) DEM is employed (Fig. 2). In high-income regions, accurately redistributing floodwater is particularly critical due to the high concentration of high-value assets and the nonlinear increase in flood damage with flooding depth. Notably, the frequency of future floods is anticipated to decrease with climate change in these regions, further diminishing the difference in EADs calculated with the two methods.

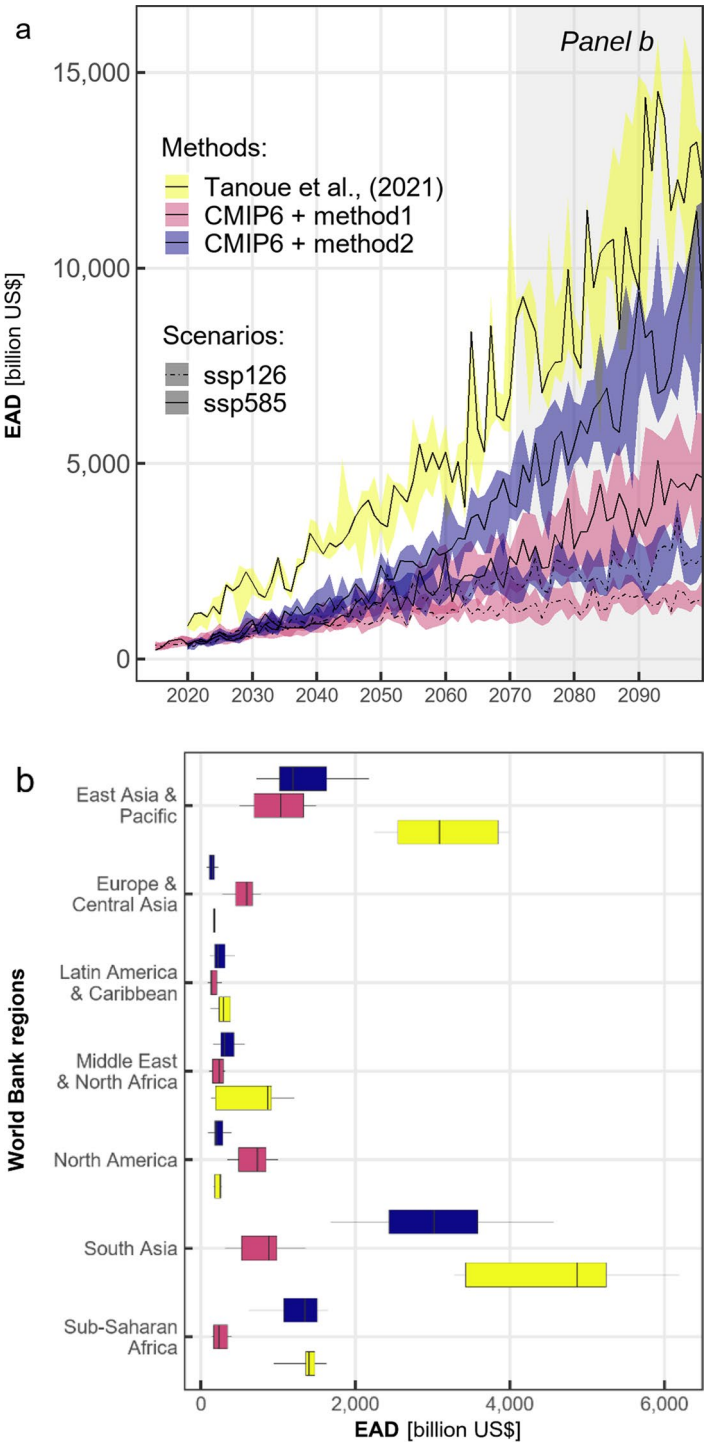
a
Panel b
15,000
10,000
5,000
0
EAD [billion US$]
Methods:
Tanoue et al., (2021)
CMIP6 + method1
CMIP6 + method2
Scenarios:
ssp126
ssp585
2020
2030
2040
2050
2060
2070
2080
2090
b
East Asia & Pacific
Europe & Central Asia
Latin America & Caribbean
Middle East & North Africa
North America
South Asia
Sub-Saharan Africa
World Bank regions
0
2,000
4,000
6,000
EAD [billion US$]

Fig. 4 Expected annual damage (EAD) under a portfolio of future flood protections. EAD are computed for ▶ different levels of adaptation, two flood damage methodologies and aggregated for the seven World Bank regions. The results for the ssp585 scenario are shown. The top red line represents the scenario with no further adaptation (setting $L=0$) and results are hence analogue to those given in Fig. 1a at the global scale

3.2 Mitigation of future flood damage under a portfolio of adaptation measures

The effects of a portfolio of future flood protection measures on future EAD are provided in Fig. 4 for the seven World Bank regions. The construction period required to complete or upgrade existing flood protections was set to 30 years. Hence, future EADs until 2050 for all regions were identical under all scenarios of the adaptation portfolio (Fig. 4). After 2050, increasing levels of flood protections (Sect. 2.4) generally reduced EAD, although the extent of this reduction varied greatly among regions. Considering the most ambitious protection scenario, the average annual benefits (between 2071 and 2100, minimum and maximum values across all regions) were $167–705 and $151–2,287 billion per year for methods 1 and 2, respectively (Fig. 4). The two flood damage methodologies produced the largest differences over South Asia and Sub-Saharan Africa under the high-emissions scenario (Fig. 4 and Supplementary Fig. 8). Under the low-emissions scenario, the ranges of EADs predicted using the two methods were generally similar in a given region. Consistent across emissions scenarios, increasing the level of flood protection tended to reduce these differences in EAD, reconciling the EAD estimates obtained with the two methods (Supplementary Fig. 9).

The difference in EADs computed using the two methods directly affected the cost–benefit analysis used to determine optimal future flood protection strategies. On average across all administrative units, optimal levels of flood protection reached 65.2 and 91.7 years with method 1 under ssp126 and ssp585, respectively. Employing method 2, optimal levels of flood protection were slightly lower than the estimates from method 1 at 57.3 and 82.7 years under ssp126 and ssp585, respectively. At the administrative level, the results were more complex (Fig. 5 and Supplementary Fig. 10). For example, under the high-emissions scenario, notably higher optimal levels of future flood protection in South Asia, East Asia and Pacific, and Sub-Saharan Africa regions were obtained using method 2 than method 1 (brown areas in Fig. 5c). These trends are consistent with the results discussed for EAD (Fig. 3b) discussed above, which is central to the cost–benefit analysis used to determine future levels of flood protection (Sect. 2.4). Note that the current levels of flood protection in these regions are uncertain and the low levels of protection included in FLOPROS may magnify the difference between optimal flood protection levels obtained with the two methods. In regions where the estimated EADs are lower with method 2 than method 1 (i.e., Europe and Central Asia, North America; see Fig. 3b), future levels of flood protection were slightly higher in the analysis relying on method 1, and the reverse was true for regions in which method 1 produced lower EADs. With climate change, some regions in Europe and Central North America will experience a decrease in flood frequency (Hirabayashi et al. 2013, 2021b), and thus increasing the level of existing flood protection may be justified only in cases of extreme GDP growth, while optimal levels of flood protection generally remain close to current levels of flood protection (Supplementary Fig. 6). Optimal levels of flood protection were lower under the low-emissions scenario (Supplementary Fig. 10) than the high-emissions scenario due to a gentler increase in flood frequency and slower increase in GDP per capita compared to the high-emissions scenario (Supplementary Fig. 7). Nevertheless, the spatial pattern of the difference in optimal flood

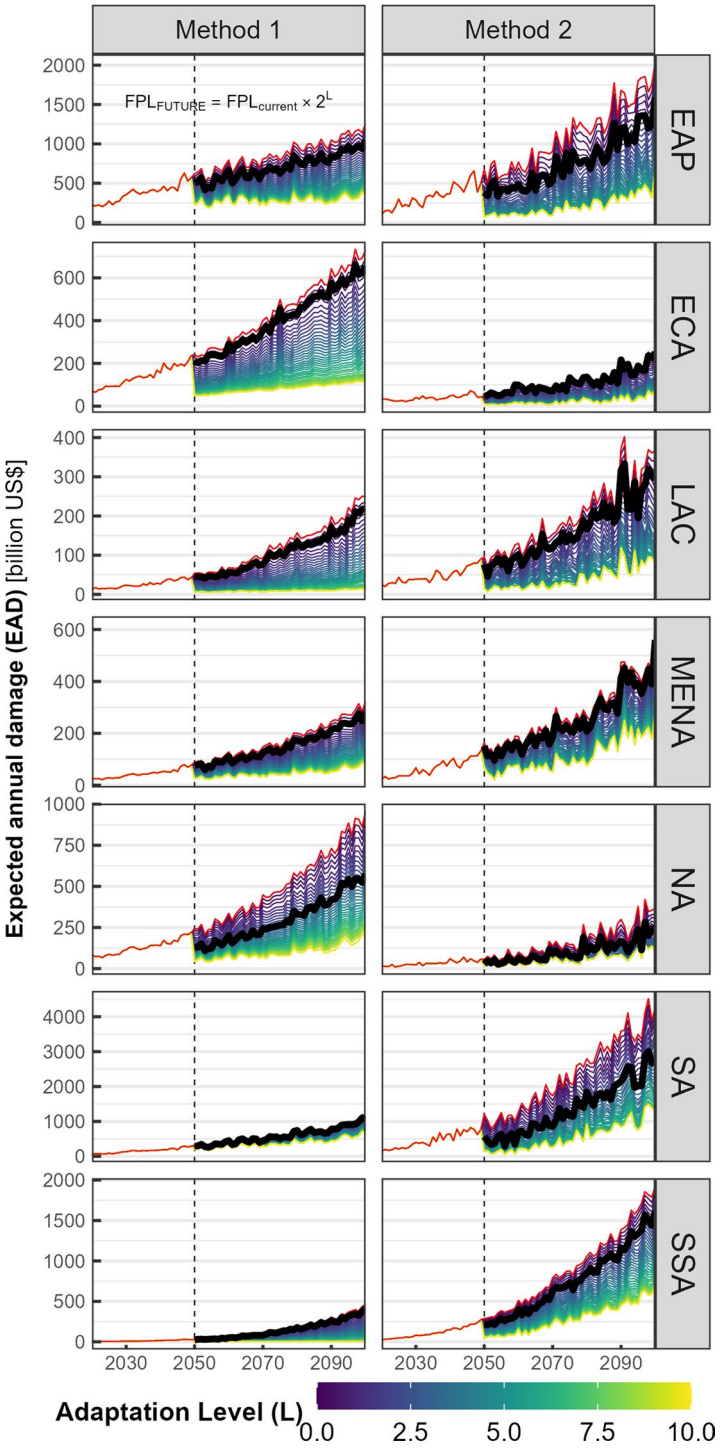
Method 1
Method 2
EAP
ECA
LAC
MENA
NA
SA
SSA
$FPL_{FUTURE} = FPL_{current} \times 2^{L}$
Expected annual damage (EAD) [billion US$]
2030
2050
2070
2090
Adaptation Level (L)
0.0
2.5
5.0
7.5
10.0

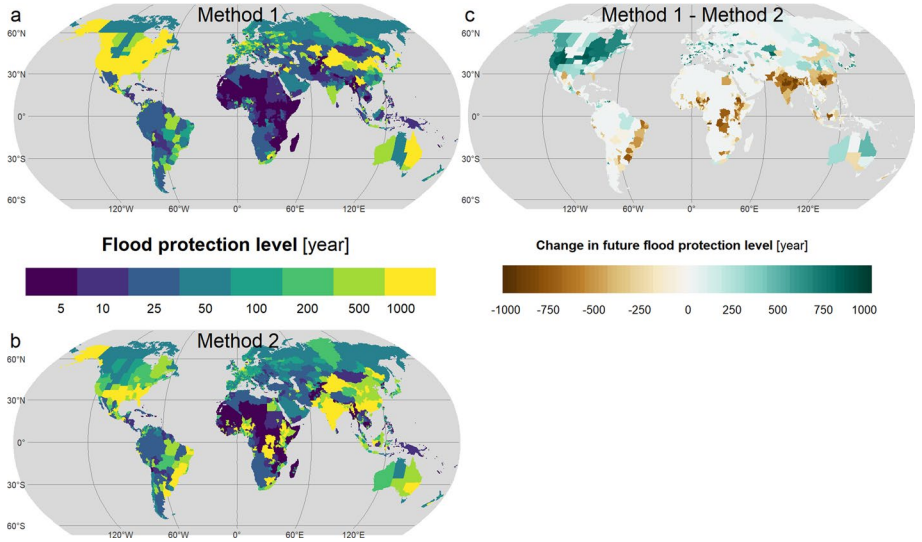

Fig. 5 Optimum future flood protection levels determined through the cost–benefit analysis. The results for the ssp585 scenario are given for **a** method 1, **b** method 2, and **c** the difference in future flood protection levels between method 1 and method 2

Table 1 Summary of global evaluation (All values in US$ billion yr^{-1})

	RDF†	Benefit	Adaptation cost	Cost-effectiveness
ssp126				
Method 1	25.8	11.6	5.3	2.2
Method 2	59.6	61.1	14.5	4.2
ssp585				
Tanoue et al., (2021)	24.3	74.0	6.8	10.8
Method1	36.2	30.0	11.0	2.7
Method2	93.2	112.0	19.0	5.9

†Under optimum flood protection level

protections between methods 1 and 2 (Supplementary Fig. 10c) is strikingly similar to the pattern obtained under the high-emissions scenario (Fig. 5c).

3.3 Residual flood risk under the optimal flood adaptation scenario

Adopting optimal levels of flood protection do not fully mitigate all flood events. On average, global RFDs were equal to $36.2 and 93.2 billion yr^{-1} under ssp585 for methods 1 and 2, respectively (Table 1). Consistent with the literature (Tanoue et al. 2021), RFDs remained high under ssp126, as future floods were predicted to cost $25.8 and 59.6 billion yr^{-1} with methods 1 and 2, respectively. These results are driven by changes in both flood frequency and future economic development (GDP), the latter of which increases linearly

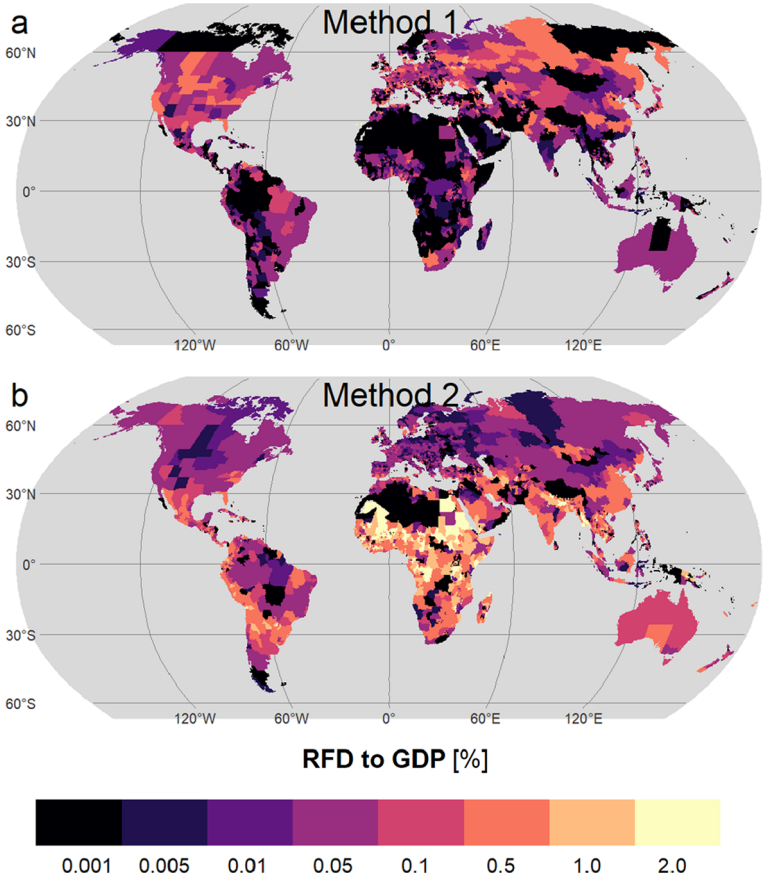

Fig. 6 RDF as a proportion of the subnational administrative GDP for the optimized adaptation objective. The result for the SSP585 scenario are shown for **a** method 1, and **b** method 2

and exponentially under the low- and high-emissions scenarios, respectively (Supplementary Fig. 7). The importance of economic development cannot be overstated, as multiple analyses suggest that socioeconomic changes, rather than climate change, will drive future impacts on water, biodiversity, energy, and other factors (Schewe et al. 2014; Dobson et al. 2021). At the global scale, the benefit, adaptation cost, and RFD values obtained using method 2 were systematically higher than the corresponding values obtained with method 1 (Table 1), consistent with the results for EAD (Fig. 4) and optimal flood protection level (Fig. 5). The importance of the gradual increase in GDP and projected intensification of flood intensity will increase greatly when future protection levels are considered, magnifying the effect of including all floodwater versus only overflow floodwater. Consequently, future EAD and RFD values predicted using method 2 are higher than those obtained with method 1 and these differences tend to increase over time.

The proportion of administrative units experiencing high RFDs (> 0.05% of subnational administrative GDP) increases sharply with the switch from method 1 to method 2 (Fig. 6 and Supplementary Fig. 11). We found that 23.3% (16.9%) of all administrative units experienced high RFDs under method 1, which would increase to 43.1% (38.0%) for method

2, under the high-emissions (low-emissions) scenario. Most administrative units exhibiting low RFDs under method 1 and large RFDs under method 2 were located in Africa (Fig. 6b), where current levels of flood protection are assumed to be low. In Central Africa, optimal levels of flood protection are, on average, 25.7 and 39.3 years higher for method 2 than method 1 under the low- and high-emissions scenarios, respectively (Fig. 5 and Supplementary Fig. 9). Despite these enhanced levels of flood protection, the high EADs predicted with method 2 explain the difference in RFDs between the two methods. A similar situation appears over the South Asia and East Asia and Pacific regions. Over arid regions of Africa, optimal levels of flood protections obtained using methods 1 and 2 are identical. This result arises because, from the perspective of cost–benefit analysis, high levels of flood protection are not justified to mitigate rare flood events (Hirabayashi et al. 2013, 2021b) given the relatively low administrative-level GDP. The North America and Europe and Central Asia regions show the opposite trend: the RFDs obtained with method 2 average 56.3 and 45.1% lower than the corresponding values obtained with method 1 under the low- and high-emissions scenarios, respectively. In these high-income and upper-middle-income economies, relatively high levels of flood protection are already available. In addition, some important economic areas are anticipated to experience decreases in flood frequency. Overall, in these regions, adjustment of EAD for future GDP conditions (i.e.,

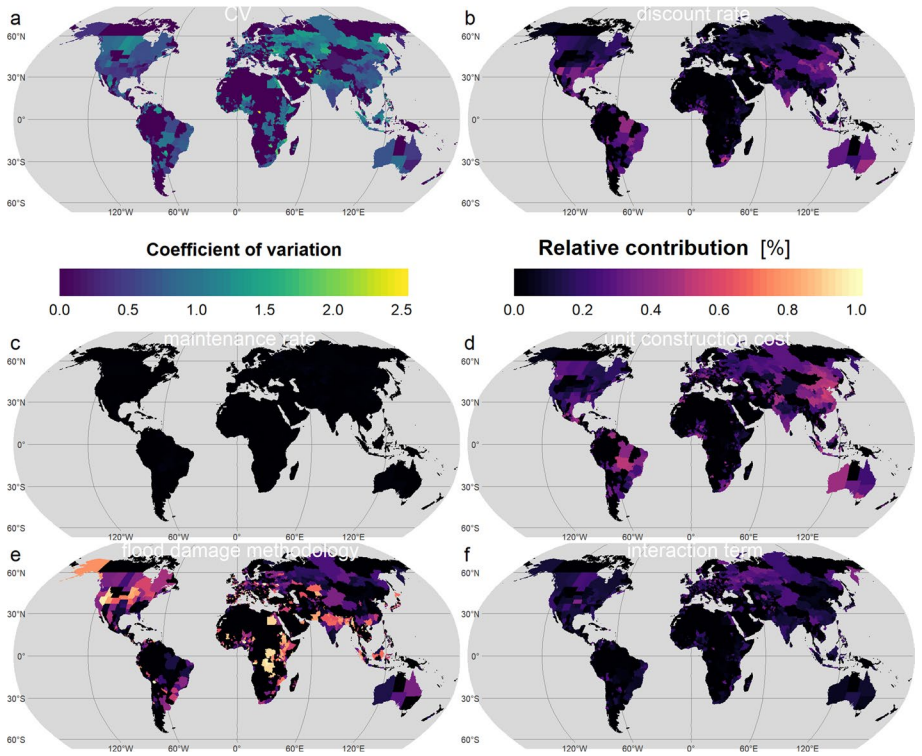

Fig. 7 Effect of cascading uncertainty for determining optimum levels of flood protections. **a** The overall variance, calculated as the fraction of standard deviation to the ensemble mean. **b–f**) The contribution rate of discount rate, maintenance cost, unit cost, flood damage methodology, and interaction term between discount rate and maintenance cost upon the overall variance

keeping the GDP spatial distribution constant at the 2010 level and correcting for future intensity only at the subnational level) and selection of a high-resolution DEM are the primary factors explaining differences in EAD and RFD between the two methods. These two factors outweigh the overflow (method 1) and all (method 2) floodwater assumptions that explain the differences in EAD and RFD in other regions (Figs. 2 and 3).

3.4 Relative importance of the flood damage methodology

In a previous analysis of residual flood damage under an intensive adaptation scenario, Tanoue et al. (2021) reported that their results were generally robust to various assumptions of discount rate, construction period, and unit construction cost. However that study did not investigate the relative importance of such factors at the administrative level and their analysis was restricted to a single method of estimating flood damage.

We report the spatial distribution of overall variance, presented as the standard deviation as a fraction of the ensemble mean optimal flood protection level (Fig. 7a and Supplementary Fig. 12a). Averaged across administrative regions, the variance was similar between emissions scenarios, at 0.32 and 0.31 under the low- and high-emissions scenarios, respectively. Notably, the variance is null across some regions of North and Central Africa, indicating that optimal levels of flood protection are insensitive tested main factors in such regions. This result suggests that, despite consideration of alternative estimates for the cost and maintenance of flood protection structures (Supplementary Table 2), the cost of building and upgrading flood protection remains unachievable, highlighting the necessity of a country-specific unit cost database (Tanoue et al. 2021). Nevertheless, the variance in optimal levels of flood protection, attributable to the four main factors is large over most of North America, Europe, Central Asia, Southeast Asia, and East Asia.

The contribution rates of each main factor and one interaction term to the overall variance (Sect. 2.5), at the administrative level were estimated using four-way ANOVA (Fig. 7b–f and Supplementary Fig. 12b–f). Consistent across emissions scenarios and administrative zones, changing the cost of maintenance only marginally impacted the derivation of optimal flood protections as its average contributions to total variance were only 1.5% and 1.1% under the low- and high-emissions scenarios, respectively (Fig. 7c). In contrast, the flood damage methodology contributed to the largest fraction of the overall variance under both the low- and high-emissions scenarios, averaging 31.3% and 38.2%, respectively (Fig. 7e). Clearly, in Alaska, Congo, Egypt, and multiple administrative regions of East Africa, the optimal level of flood protection was driven solely by the flood damage methodology, which had a relative contribution to total variance of nearly one. As noted above, this result is due to the use of only overflow water or all floodwater, the use of different high-resolution DEMs for downscaling, and different spatial distributions of future GDP. Notably, these factors affect developing and high-income economies differently. The spatial distributions of the relative contribution rates of the discount rate and unit construction cost under the two emissions scenarios are similar. The contributions to overall variance of the discount rate and unit construction cost are relatively high, averaging 12.4% and 22.3% under the low-emissions scenario and 14.8 and 19.6% under the high-emissions scenario, respectively (Fig. 7b and d). Their spatial distributions are also similar, particularly over Central Asia, East Asia, and South America, where the contributions of discount rate, unit construction cost, and flood damage method are similar.

Our results show low contributions of interaction terms (both first- and second-order terms). One notable exception is the third-order interaction term (Fig. 7f and Supplementary Fig. 12f), which averaged 15.2% and 12.8% of total variance under the low- and

Table 2 The average contribution rates (in %) of the discount rate, maintenance cost, unit construction cost, flood damage methodology, and third interaction term on the overall variance across all seven World Bank regions (EAP: East Asia and Pacific, ECA: Europe and Central Asia, LAC: Latin America and Caribbean, MENA: Middle East and North Africa, NA: North America, SA: South Asia, SSA: Sub-Saharan Africa) are presented for both ssp126 and ssp585 scenarios

WB regions	EAP	ECA	LAC	MENA	NA	SA	SSA
ssp126							
Discount rate	13.0	8.4	17.5	11.9	13.1	14.1	10.6
Maintenance rate	1.2	0.8	1.4	1.1	0.8	1.2	0.9
Unit construction cost	26.1	16.8	30.0	21.8	19.6	23.8	16.8
Flood damage meth	38.6	47.0	30.2	40.0	44.9	42.9	54.2
Interaction term	13.1	18.3	13.1	17.0	13.7	12.9	12.2
ssp585							
Discount rate	17.7	10.2	19.5	13.3	17.3	19.9	16.2
Maintenance rate	1.0	0.7	1.0	0.8	0.6	0.7	0.8
Unit construction cost	23.2	15.6	22.6	17.9	15.7	16.5	18.0
Flood damage meth	37.9	51.7	38.2	43.9	45.6	52.0	50.0
Interaction term	12.5	14.5	11.8	16.0	12.0	10.5	10.1

high-emissions scenario, respectively. Discount rate generally affects EAD, optimal flood protection, and RFD results through maintenance costs, and this impact is particularly pronounced over eastern North America and some administrative regions of China and Russia. The significant influence of the flood damage methodology selected on overall variance is clear across all World Bank regions (Table 2). Interestingly, in the regions of East Asia and Pacific and Latin America and Caribbean, the unit construction cost has a comparable influence to flood damage methodology on determination of the optimal flood protection level. Additionally, the switch from the low-emissions to high-emissions scenario increased the contribution of the discount rate to overall variance in all regions.

4 Conclusion

Using an updated global river and inundation model based on accurate topography and forced by the lasted climate simulations, we quantified changes in EAD from flooding, optimal levels of flood protection, and RFD while considering two established flood damage methodologies and key economic assumptions.

In the future, assuming current levels of flood protection, global EAD will increase sharply by $16.2 and $44.5 billion per year under a low- and high-emissions scenarios, respectively. However, these estimates approximately double when an alternative flood damage methodology is used, reaching $31.1 and $90.3 billion per year under the low- and high-emissions scenarios, respectively. The uncertainty in EAD estimates cascades down to the estimation of optimal flood protection level, which is determined through cost–benefit analysis. Compared to current levels of flood protection, optimal levels of flood protection will increase by 35.5 and 62.1 years under the low- and high-emissions scenarios, respectively. Using the alternative methodology for determining flood damage, these optimal levels of flood protection were approximately 10 years shorter under both emissions scenarios. Uncertainties in optimal levels of flood protection further propagate to the

calculation of RFDs, which differ by an average of $45.4 billion per year between flood damage methodologies.

ANOVA results were consistent across emissions scenarios, and flood damage methodology was identified as the dominant source of uncertainty in an average of 18.0% of the 3,508 administrative units. Uncertainties due to flood damage methodology arise mainly from three mechanisms: reliance on either floodplain or overflow floodwater for estimation of flooded area, selection of a high-resolution DEM for downscaling of data, and adjustment of future GDP levels at the administrative scale. Critically, these mechanisms have contrasting impacts on developing and high-income economies. Economic assumptions about unit construction cost and discount rate still play an important role in determining optimal flood protections measures, explaining at least 20% of the total variance in an average of 17.5% of all administrative units. In these administrative units, the uncertainty stemming from the flood damage methodology selected is not disproportionately high compared to the uncertainties of key economic assumptions; therefore, the less resource-intensive flood damage methodology (method 2) is not detrimental to the quality of analysis in such areas. Notably, variance in the optimal level of flood protection was null for approximately 66.3% of all administrative units, principally located in Africa and Latin America. This finding indicates that the range of economic assumptions considered in this study may not reflect the unit construction costs and advantageous discount rates available in these regions. While acquiring realistic data for these regions should be a research priority, our findings emphasize the need for cooperative frameworks that will support adaptation to future flood risk.

Supplementary Information The online version contains supplementary material available at https://doi.org/10.1007/s11069-023-06017-7.

Authors contributions Flood simulations were mainly conducted by YT and completed by BJ. All authors contributed to the study conception and design. Material preparation, data collection and analysis were performed by BJ, TM and YT. The first draft of the manuscript was written by BJ, and all authors commented on previous versions of the manuscript. All authors read and approved the final manuscript.

Funding This research was supported by the Environment Research and Technology Development Fund (JPMEERF20202005) of the Environmental Restoration and Conservation Agency of Japan, NEDO project (JP21500379), and SOUHATSU project (JPMJFR215P) from the Ministry of Education, Culture, Sports, Science and Technology (MEXT), Japan.

Data availability Raw data were generated at Shibaura Institute of Technology and are available from B. J. and H. Y. upon reasonable request. All scripts used to analyze the data and prepare the figures and tables are openly available in Zenodo https://doi.org/10.5281/zenodo.7214273.

Declarations

Conflict of interest The authors have no relevant financial or non-financial interests to disclose.

References

Alfieri L, Bisselink B, Dottori F et al (2017) Global projections of river flood risk in a warmer world. Earths Future 5:171–182. https://doi.org/10.1002/2016EF000485

Arrighi C, Campo L (2019) Effects of digital terrain model uncertainties on high-resolution urban flood damage assessment. J Flood Risk Manag 12:e12530. https://doi.org/10.1111/jfr3.12530

Bates PD, Horritt MS, Fewtrell TJ (2010) A simple inertial formulation of the shallow water equations for efficient two-dimensional flood inundation modelling. J Hydrol 387:33–45. https://doi.org/10.1016/j.jhydrol.2010.03.027

Bevacqua E, Maraun D, Vousdoukas MI et al (2019) Higher probability of compound flooding from precipitation and storm surge in Europe under anthropogenic climate change. Sci Adv 5:eaww5531. https://doi.org/10.1126/sciadv.aaw5531

Blöschl G, Hall J, Viglione A et al (2019) Changing climate both increases and decreases European river floods. Nature 573:108–111. https://doi.org/10.1038/s41586-019-1495-6

Boulange J, Hanasaki N, Yamazaki D, Pokhrel Y (2021) Role of dams in reducing global flood exposure under climate change. Nat Commun 12:417. https://doi.org/10.1038/s41467-020-20704-0

Campbell S, Remenyi TA, White CJ, Johnston FH (2018) Heatwave and health impact research: a global review. Health Place 53:210–218. https://doi.org/10.1016/j.healthplace.2018.08.017

Chaudhari S, Pokhrel Y (2022) Alteration of River Flow and Flood Dynamics by Existing and Planned Hydropower Dams in the Amazon River Basin. Water Resour Res 58:e202WR1030555. https://doi.org/10.1029/2021WR030555

Chavez-Demoulin V, Davison AC (2012) Modelling time series extremes. REVSTAT - Stat J 10:109

D'Ippoliti D, Michelozzi P, Marino C et al (2010) The impact of heat waves on mortality in 9 European cities: results from the EuroHEAT project. Environ Health 9:37. https://doi.org/10.1186/1476-069X-9-37

Davenport FV, Burke M, Diffenbaugh NS (2021) Contribution of historical precipitation change to US flood damages. Proc Natl Acad Sci 118:e2017524118. https://doi.org/10.1073/pnas.2017524118

Devitt L, Neal J, Wagener T, Coxon G (2021) Uncertainty in the extreme flood magnitude estimates of large-scale flood hazard models. Environ Res Lett 16:064013. https://doi.org/10.1088/1748-9326/abfac4

Díez-Herrero A, Garrote J (2020) Flood risk analysis and assessment, applications and uncertainties: a bibliometric Review. Water 12:2050. https://doi.org/10.3390/w12072050

Dobson A, Rowe Z, Berger J et al (2021) Biodiversity loss due to more than climate change. Science 374:699–700. https://doi.org/10.1126/science.abm6216

Dong S, Sun Y, Li C et al (2021) Attribution of extreme precipitation with updated observations and CMIP6 simulations. J Clim 34:871–881. https://doi.org/10.1175/JCLI-D-19-1017.1

Dottori F, Szewczyk W, Ciscar J-C et al (2018) Increased human and economic losses from river flooding with anthropogenic warming. Nat Clim Change 8:781–786. https://doi.org/10.1038/s41558-018-0257-z

Dottori F, Mentaschi L, Bianchi A et al (2023) Cost-effective adaptation strategies to rising river flood risk in Europe. Nat Clim Change 13:196–202. https://doi.org/10.1038/s41558-022-01540-0

Du S, Scussolini P, Ward PJ et al (2020) Hard or soft flood adaptation? Advantages of a hybrid strategy for Shanghai. Glob Environ Change 61:102037. https://doi.org/10.1016/j.gloenvcha.2020.102037

Eilander D, van Verseveld W, Yamazaki D et al (2021) A hydrography upscaling method for scale-invariant parametrization of distributed hydrological models. Hydrol Earth Syst Sci 25:5287–5313. https://doi.org/10.5194/hess-25-5287-2021

Eyring V, Bony S, Meehl GA et al (2016) Overview of the coupled model intercomparison project phase 6 (CMIP6) experimental design and organization. Geosci Model Dev 9:1937–1958. https://doi.org/10.5194/gmd-9-1937-2016

Getirana A, Kumar SV, Konapala G, Ndehedehe CE (2021) Impacts of fully coupling land surface and flood models on the simulation of large wetlands' water dynamics: the case of the inner Niger Delta. J Adv Model Earth Syst 13:e2021MS002463. https://doi.org/10.1029/2021MS002463

Greenwood JA, Landwehr JM, Matalas NC, Wallis JR (1979) Probability weighted moments: Definition and relation to parameters of several distributions expressable in inverse form. Water Resour Res 15:1049–1054. https://doi.org/10.1029/WR015i005p01049

Gumbel EJ (1941) The return period of flood flows. Ann Math Stat 12:163–190

Hallegatte S, Green C, Nicholls RJ, Corfee-Morlot J (2013) Future flood losses in major coastal cities. Nat Clim Change 3:802–806. https://doi.org/10.1038/nclimate1979

Hanazaki R, Yamazaki D, Yoshimura K (2022) Development of a reservoir flood control scheme for global flood models. J Adv Model Earth Syst 14:e2021MS002944. https://doi.org/10.1029/2021MS002944

Harada Y, Kamahori H, Kobayashi C et al (2016) The JRA-55 reanalysis: representation of atmospheric circulation and climate variability. J Meteorol Soc Jpn Ser II 94:269–302. https://doi.org/10.2151/jmsj.2016-015

Hattermann FF, Vetter T, Breuer L et al (2018) Sources of uncertainty in hydrological climate impact assessment: a cross-scale study. Environ Res Lett 13:015006. https://doi.org/10.1088/1748-9326/aa9938

Hirabayashi Y, Mahendran R, Koirala S et al (2013) Global flood risk under climate change. Nat Clim Change 3:816–821. https://doi.org/10.1038/nclimate1911

Hirabayashi Y, Alifu H, Yamazaki D et al (2021a) Anthropogenic climate change has changed frequency of past flood during 2010-2013. Prog Earth Planet Sci 8:36. https://doi.org/10.1186/s40645-021-00431-w

Hirabayashi Y, Tanoue M, Sasaki O et al (2021b) Global exposure to flooding from the new CMIP6 climate model projections. Sci Rep 11:3740. https://doi.org/10.1038/s41598-021-83279-w

Hosking JRM, Wallis JR (1997) Regional Frequency Analysis: An Approach Based on L-Moments. Cambridge University Press, Cambridge

Huizinga J, de Moel H, Szewcyk W (2017) Global flood depth-damage functions: Methodology and the database with guidelines. https://doi.org/10.2760/16510

Iizumi T, Takikawa H, Hirabayashi Y et al (2017) Contributions of different bias-correction methods and reference meteorological forcing data sets to uncertainty in projected temperature and precipitation extremes. J Geophys Res Atmos 122:7800–7819. https://doi.org/10.1002/2017JD026613

Johnson KA, Wing OEJ, Bates PD et al (2020) A benefit–cost analysis of floodplain land acquisition for US flood damage reduction. Nat Sustain 3:56–62. https://doi.org/10.1038/s41893-019-0437-5

Jongman B, Ward PJ, Aerts JCJH (2012) Global exposure to river and coastal flooding: Long term trends and changes. Glob Environ Change 22:823–835. https://doi.org/10.1016/j.gloenvcha.2012.07.004

Jongman B, Hochrainer-Stigler S, Feyen L et al (2014) Increasing stress on disaster-risk finance due to large floods. Nat Clim Change 4:264–268. https://doi.org/10.1038/nclimate2124

Kelley CP, Mohtadi S, Cane MA et al (2015) Climate change in the Fertile Crescent and implications of the recent Syrian drought. Proc Natl Acad Sci 112:3241–3246. https://doi.org/10.1073/pnas.1421533112

Kinoshita Y, Tanoue M, Watanabe S, Hirabayashi Y (2018) Quantifying the effect of autonomous adaptation to global river flood projections: application to future flood risk assessments. Environ Res Lett 13:014006. https://doi.org/10.1088/1748-9326/aa9401

Kirezci E, Young IR, Ranasinghe R et al (2023) Global-scale analysis of socioeconomic impacts of coastal flooding over the 21st century. Front Mar Sci 9:2808

Kulp SA, Strauss BH (2019) New elevation data triple estimates of global vulnerability to sea-level rise and coastal flooding. Nat Commun 10:4844. https://doi.org/10.1038/s41467-019-12808-z

Kundzewicz ZW, Kanae S, Seneviratne SI et al (2014) Flood risk and climate change: global and regional perspectives. Hydrol Sci J 59:1–28. https://doi.org/10.1080/02626667.2013.857411

Lewis SC, Karoly DJ (2013) Anthropogenic contributions to Australia's record summer temperatures of 2013. Geophys Res Lett 40:3705–3709. https://doi.org/10.1002/grl.50673

Lüdtke S, Schröter K, Steinhausen M et al (2019) A consistent approach for probabilistic residential flood loss modeling in Europe. Water Resour Res 55:10616–10635. https://doi.org/10.1029/2019WR026213

Mann ME, Gleick PH (2015) Climate change and California drought in the 21st century. Proc Natl Acad Sci 112:3858–3859. https://doi.org/10.1073/pnas.1503667112

Marsooli R, Lin N, Emanuel K, Feng K (2019) Climate change exacerbates hurricane flood hazards along US Atlantic and Gulf Coasts in spatially varying patterns. Nat Commun 10:3785. https://doi.org/10.1038/s41467-019-11755-z

McGrath H, Abo El Ezz A, Nastev M (2019) Probabilistic depth–damage curves for assessment of flood-induced building losses. Nat Hazards 97:1–14. https://doi.org/10.1007/s11069-019-03622-3

Mei C, Liu J, Wang H et al (2020) Urban flood inundation and damage assessment based on numerical simulations of design rainstorms with different characteristics. Sci China Technol Sci 63:2292–2304. https://doi.org/10.1007/s11431-019-1523-2

Meresa H, Murphy C, Fealy R, Golian S (2021) Uncertainties and their interaction in flood hazard assessment with climate change. Hydrol Earth Syst Sci 25:5237–5257. https://doi.org/10.5194/hess-25-5237-2021

Merz B, Kreibich H, Schwarze R, Thieken A (2010) Review article "Assessment of economic flood damage." Nat Hazards Earth Syst Sci 10:1697–1724. https://doi.org/10.5194/nhess-10-1697-2010

Molinari D, De Bruijn KM, Castillo-Rodríguez JT et al (2019) Validation of flood risk models: Current practice and possible improvements. Int J Disaster Risk Reduct 33:441–448. https://doi.org/10.1016/j.ijdrr.2018.10.022

Paik S, Min S-K, Zhang X et al (2020) Determining the Anthropogenic Greenhouse Gas Contribution to the Observed Intensification of Extreme Precipitation. Geophys Res Lett 47:e2019GL086875. https://doi.org/10.1029/2019GL086875

Pörtner H-O, Roberts DC, Poloczanska ES, et al (2022) IPCC: Summary for Policymakers. Contribution of Working Group II to the Sixth Assessment Report of the Intergovernmental Panel on Climate Change, Cambridge University Press

Rasmussen DJ, Buchanan MK, Kopp RE, Oppenheimer M (2020) A flood damage allowance framework for coastal protection with deep uncertainty in sea level rise. Earths Future 8:e2019EF001340. https://doi.org/10.1029/2019EF001340

Ritchie J, Dowlatabadi H (2017) Why do climate change scenarios return to coal? Energy 140:1276–1291. https://doi.org/10.1016/j.energy.2017.08.083

Romali NS, Yusop Z (2020) Flood damage and risk assessment for urban area in Malaysia. Hydrol Res 52:142–159. https://doi.org/10.2166/nh.2020.121

Rözer V, Kreibich H, Schröter K et al (2019) Probabilistic models significantly reduce uncertainty in hurricane harvey pluvial flood loss estimates. Earths Future 7:384–394. https://doi.org/10.1029/2018EF001074

Satoh Y, Shiogama H, Hanasaki N et al (2021) A quantitative evaluation of the issue of drought definition: a source of disagreement in future drought assessments. Environ Res Lett 16:104001. https://doi.org/10.1088/1748-9326/ac2348

Sauer IJ, Reese R, Otto C et al (2021) Climate signals in river flood damages emerge under sound regional disaggregation. Nat Commun 12:2128. https://doi.org/10.1038/s41467-021-22153-9

Schewe J, Heinke J, Gerten D et al (2014) Multimodel assessment of water scarcity under climate change. Proc Natl Acad Sci 111:3245–3250. https://doi.org/10.1073/pnas.1222460110

Scussolini P, Aerts JCJH, Jongman B et al (2016) FLOPROS: an evolving global database of flood protection standards. Nat Hazards Earth Syst Sci 16:1049–1061. https://doi.org/10.5194/nhess-16-1049-2016

Shrestha BB, Perera EDP, Kudo S et al (2019) Assessing flood disaster impacts in agriculture under climate change in the river basins of Southeast Asia. Nat Hazards 97:157–192. https://doi.org/10.1007/s11069-019-03632-1

Taguchi R, Tanoue M, Yamazaki D, Hirabayashi Y (2022) Global-scale assessment of economic losses caused by flood-related business interruption. Water 14(6):967. https://doi.org/10.3390/w14060967

Takata K, Emori S, Watanabe T (2003) Development of the minimal advanced treatments of surface interaction and runoff. Proj Intercomp Land-Surf Parameterization Sch Phase 38(1–2):209–222. https://doi.org/10.1016/S0921-8181(03)00030-4

Tanoue M, Taguchi R, Nakata S et al (2020) Estimation of direct and indirect economic losses caused by a flood with long-lasting inundation: application to the 2011 Thailand flood. Water Resour Res 56:e2019WR026092. https://doi.org/10.1029/2019WR026092

Tanoue M, Taguchi R, Alifu H, Hirabayashi Y (2021) Residual flood damage under intensive adaptation. Nat Clim Change 11:823–826. https://doi.org/10.1038/s41558-021-01158-8

Trigg MA, Birch CE, Neal JC et al (2016) The credibility challenge for global fluvial flood risk analysis. Environ Res Lett 11:094014. https://doi.org/10.1088/1748-9326/11/9/094014

Vousdoukas MI, Bouziotas D, Giardino A et al (2018a) Understanding epistemic uncertainty in large-scale coastal flood risk assessment for present and future climates. Nat Hazards Earth Syst Sci 18:2127–2142. https://doi.org/10.5194/nhess-18-2127-2018

Vousdoukas MI, Mentaschi L, Voukouvalas E et al (2018b) Global probabilistic projections of extreme sea levels show intensification of coastal flood hazard. Nat Commun 9:2360. https://doi.org/10.1038/s41467-018-04692-w

Vousdoukas MI, Mentaschi L, Voukouvalas E et al (2018c) Climatic and socioeconomic controls of future coastal flood risk in Europe. Nat Clim Change 8:776–780. https://doi.org/10.1038/s41558-018-0260-4

Ward PJ, Jongman B, Weiland FS et al (2013) Assessing flood risk at the global scale: model setup, results, and sensitivity. Environ Res Lett 8:044019. https://doi.org/10.1088/1748-9326/8/4/044019

Ward PJ, Jongman B, Aerts JCJH et al (2017) A global framework for future costs and benefits of river-flood protection in urban areas. Nat Clim Change 7:642–646. https://doi.org/10.1038/nclimate3350

Wing OEJ, Bates PD, Neal JC et al (2019) A New automated method for improved flood defense representation in large-scale hydraulic models. Water Resour Res 55:11007–11034. https://doi.org/10.1029/2019WR025957

Wing OEJ, Pinter N, Bates PD, Kousky C (2020) New insights into US flood vulnerability revealed from flood insurance big data. Nat Commun 11:1444. https://doi.org/10.1038/s41467-020-15264-2

Winsemius HC, Van Beek LPH, Jongman B et al (2013) A framework for global river flood risk assessments. Hydrol Earth Syst Sci 17:1871–1892. https://doi.org/10.5194/hess-17-1871-2013

Winsemius HC, Aerts JCJH, van Beek LPH et al (2016) Global drivers of future river flood risk. Nat Clim Change 6:381–385. https://doi.org/10.1038/nclimate2893

Xu K, Wang C, Bin L (2023) Compound flood models in coastal areas: a review of methods and uncertainty analysis. Nat Hazards 116:469–496. https://doi.org/10.1007/s11069-022-05683-3

Yamada T, Fujita R, Tanoue M et al (2021) Sensitivity experiments of global river models to different physical processes and elevation data and changes in flood risk. J Jpn Soc Civ Eng Ser G Environ Res 77:27–32. https://doi.org/10.2208/jscejer.77.5_I_27

Yamazaki D, Oki T, Kanae S (2009) Deriving a global river network map and its sub-grid topographic characteristics from a fine-resolution flow direction map. Hydrol Earth Syst Sci 13:2241–2251. https://doi.org/10.5194/hess-13-2241-2009

Yamazaki D, Kanae S, Kim H, Oki T (2011) A physically based description of floodplain inundation dynamics in a global river routing model. Water Resour Res. https://doi.org/10.1029/2010WR009726

Yamazaki D, Lee H, Alsdorf DE et al (2012) Analysis of the water level dynamics simulated by a global river model: a case study in the Amazon River. Water Resour Res. https://doi.org/10.1029/2012WR011869

Yamazaki D, Sato T, Kanae S et al (2014) Regional flood dynamics in a bifurcating mega delta simulated in a global river model. Geophys Res Lett 41:3127–3135. https://doi.org/10.1002/2014GL059744

Yamazaki D, Ikeshima D, Tawatari R et al (2017) A high-accuracy map of global terrain elevations. Geophys Res Lett 44:5844–5853. https://doi.org/10.1002/2017GL072874

Yamazaki D, Ikeshima D, Sosa J et al (2019) MERIT hydro: a high-resolution global hydrography map based on latest topography dataset. Water Resour Res 55:5053–5073. https://doi.org/10.1029/2019WR024873

Zhao F, Veldkamp TIE, Frieler K et al (2017) The critical role of the routing scheme in simulating peak river discharge in global hydrological models. Environ Res Lett 12:075003. https://doi.org/10.1088/1748-9326/aa7250

Zhou X, Ma W, Echizenya W, Yamazaki D (2021) The uncertainty of flood frequency analyses in hydrodynamic model simulations. Nat Hazards Earth Syst Sci 21:1071–1085. https://doi.org/10.5194/nhess-21-1071-2021